

# An Edible Bistable Tilt Sensor Enabling Autonomous Operation of a Partially Eatable Rolling Robot

Valerio F. Annese,\* Bokeon Kwak, Giulia Coco, Valerio Galli, Ivan K. Ilic, Pietro Cataldi, Dario Floreano,\* and Mario Caironi\*

Edible electronics and robotics are emerging areas intimately bridging food science and engineering to deliver technology using food-derived materials. Edible devices offer unprecedented opportunities thanks to features such as bioresorbability, nutritional value, associated taste, minimal toxicity, and sustainability. However, several challenges need to be addressed to bring edible devices closer to reality. Although prototypal edible sensors are available, rotation sensors—an essential component for orientation perception—are still missing. Integrating sensors, actuators, and structural components into an edible system also remains a challenge due to the lack of processes and standardization. Here the first edible tilt sensor is presented. Starting from a commercial nonedible bistable tilt sensor, each material is replaced with edible equivalents using simple and straightforward fabrication approaches. Its functionality is validated in the first implementation of an autonomous and partly edible rolling robot, which has a nutritional value of 807.5 kcal and integrates gelatin actuators, an array of tilt sensors, and an edible wheeled frame. The robot works in closed loop, perceiving its orientation and input for actuation from the sensors. These findings may pave the way to novel edible technologies, from drug delivery for wild animals to health applications.

e-waste accumulate in the environment globally,<sup>[3]</sup> which is a weight equivalent to 109 Empire State Buildings.<sup>[4]</sup> The e-waste accumulation has numerous adverse effects on the entire globe, including heavy metals and toxic chemicals release, soil contamination, irreversible damage to flora and fauna, biohazard, and climate change, ultimately threatening the health of wild animals and humans.<sup>[5]</sup> Furthermore, electronic and robotic components are made with a variety of materials with different disposal requirements, resulting in a complicated recycling stream.<sup>[6]</sup> Therefore, action is needed to address concerns about the end of the lifecycle of robots and electronics.

Edible electronics is a rapidly growing research field aiming at delivering electronic components made of foodstuff and food-derived materials, potentially integrable into more complex systems such as edible robots, with the vision of delivering next-generation sustainable technologies.<sup>[7–9]</sup> The use of safe-to-eat

materials to deliver electronics and robotics has unique features over conventional implementations; edible systems are not only biodegradable, biocompatible, and environmentally sustainable, but they also employ materials with minimal toxicity levels, especially in case of accidental or voluntary ingestion by humans or wild animals. These advantages open unprecedented application scenarios. For instance, edible sensors can be employed in


## 1. Introduction

As society progress toward automation where the use of robots will soon be pervasive, the accumulation of electronic waste (e-waste) in the environment and wastewater represents a major and ever-growing problem.<sup>[1,2]</sup> Every year, 40 million tons of

V. F. Annese, G. Coco, V. Galli, I. K. Ilic, P. Cataldi, M. Caironi  
Center for Nano Science and Technology  
Istituto Italiano di Tecnologia  
Via Rubattino 81, Milan 20134, Italy  
E-mail: valerio.annese@iit.it; mario.caironi@iit.it

B. Kwak, D. Floreano  
Laboratory of Intelligent Systems  
École Polytechnique Fédérale de Lausanne (EPFL)  
Lausanne 1015, Switzerland  
E-mail: dario.floreano@epfl.ch

G. Coco, V. Galli  
Department of Physics  
Politecnico di Milano  
Piazza Leonardo da Vinci, 32, Milan 20133, Italy  
P. Cataldi  
Smart Materials  
Istituto Italiano di Tecnologia  
Via Morego 30, Genoa 16163, Italy

 The ORCID identification number(s) for the author(s) of this article can be found under <https://doi.org/10.1002/adrs.202300092>

© 2023 The Authors. Advanced Sensor Research published by Wiley-VCH GmbH. This is an open access article under the terms of the Creative Commons Attribution License, which permits use, distribution and reproduction in any medium, provided the original work is properly cited.

DOI: 10.1002/adrs.202300092

applications requiring direct food contact since possible residues are of no safety concern.<sup>[10]</sup> Also, the locomotion abilities and the associated taste of an artificial prey could be leveraged as robotic food acting as vectors for controlled drug delivery in wild and endangered animals. Ultimately, edible technologies could be advantageous for gastrointestinal (GI) tract monitoring, overcoming the current retention risks and pioneer a new class of non-invasive diagnostic tools that are degraded within the body (e.g., digested or even metabolized) after completing their task. Edible circuits and components also have an associated nutritional value, an unparalleled feature of any conventional device. The inherent delivery of nutrients can be leveraged in rescue missions, where edible robots could effectively remove the need for food payloads.<sup>[11]</sup> At the end of their lifecycle, edible electronics and robots could be disposed of in various sustainable ways, including repurposing for animal feed and insect farming or production of compost, biogas, biofuel, and bioplastics. As such, edible technologies overcome some emerging limitations of biodegradable ones, which are designed to degrade over time.<sup>[12–23]</sup> For example, some large-scale produced bioplastics, such as polylactic acid, remain a potential life threat when left in the environment before their complete degradation, especially in case of ingestion by wild animals.<sup>[11]</sup> Also, there are concerns that biodegradable polymers could release in the environment slowly degradable micro- and nano-plastics, which have recently been detected in human blood<sup>[24]</sup> with debated consequences.<sup>[25,26]</sup>

Edible electronic components have already been documented in the literature,<sup>[27–34]</sup> including conductors,<sup>[27]</sup> resistors,<sup>[27]</sup> capacitors,<sup>[28]</sup> transistors,<sup>[29]</sup> memristors,<sup>[30,31]</sup> resonators,<sup>[32]</sup> and power sources.<sup>[33,34]</sup> Similarly, the development of edible sensors is making progress, with working edible prototypes successfully implemented such as impedance,<sup>[35]</sup> strain,<sup>[36,37]</sup> pH,<sup>[38]</sup> and piezoelectric<sup>[39]</sup> sensors. Edible sensors have also been used for food quality monitoring<sup>[10,38,40]</sup> and biomedical applications.<sup>[41–43]</sup> So far, no edible tilt sensor, a key component in any rotation system, has been documented yet. In robotics, edible actuators have also been developed,<sup>[7,8,17,44–46]</sup> for instance, using hydrogels,<sup>[8,17,23,44,45]</sup> commercial candies,<sup>[46]</sup> and popcorn kernels.<sup>[7]</sup> A few edible robots have also been demonstrated so far.<sup>[9,11,13]</sup> However, these prototypes do not integrate edible sensors and actuators. As such, none of these edible robots display autonomous operation. For instance, one of the first edible robots uses rolling for locomotion by differentially inflating two gelatin actuators powered by a chemical reaction generating gas.<sup>[9]</sup> However, the robot does not integrate sensors; therefore, it only works in open loop (similar rolling robots<sup>[47–58]</sup> have been reviewed in Table S1 in the Supporting Information). A closed-loop control system with sensors for state perception is necessary to enable autonomous operation in edible robotics.

Here we present the first edible tilt sensor. The sensor herein presented is a bistable resistive component. It emulates a commercial version in an edible format by leveraging food-grade gold laminated onto ethyl cellulose as electrodes, an activated carbon-based oleogel as a conductive element, and a gelatin capsule as an encapsulant. To demonstrate its functionality in edible robotics, we have integrated a circular array of six edible tilt sensors into a partially edible rolling robot. The robot features an edible wheel structure that hosts six gelatin actuators. Our implementation represents the first integration of edible sensors, edible actuators,

and edible structural components into the same autonomous system. Using data from the edible sensors, the robot can autonomously identify its orientation, activate the correct actuator to sustain rolling motion, detect forward and backward movement, and ultimately detect falls or inconsistent orientation. The materials and methods herein developed have a high degree of versatility and can be applied to a variety of application scenarios, such as ingestible technologies for health applications, entertainment, and robotic food.<sup>[59]</sup>

## 2. Edible Tilt Sensor

A bistable resistive tilt sensor, also referred to as a tilt switch or electrical contact sensor, consists of two conducting electrodes and an electrically conductive mass that can freely move in a cavity (Figure 1a). When the sensor is tilted in the appropriate direction, the conductive mass connects the electrodes, thus closing an electrical circuit (state ON). Tilting the sensor in the opposite direction moves the mass away from the contacts, thus opening the circuit (state OFF). Bistable tilt sensors represent the simplest rotation sensors available on the market. Although bistable sensors cannot provide a precise reading of the rotation angle, they are advantageous because they can be operated in direct current, are robust, low-cost, simple, durable, reliable, lightweight, and do not require amplification, filtering, or calibration.<sup>[60]</sup> Furthermore, an array of suitably oriented bistable sensors could approximate the rotational angle of a device.

The fully edible implementation of the bistable resistive sensor was achieved using only food-grade materials, ingestible in large amounts without toxic adverse effects (Figure 1b; Figure S1a,b, Supporting Information). Specifically, the electrically conductive mass was obtained by melt-mixing beeswax (E 901) and sunflower oil in a 3:1 w:w ratio and loading the oleogel with 30% in weight of activated carbon (E 153). Activated carbon is an electronic conductor and can be consumed in relatively large amounts ( $\geq 500$  mg kg<sup>−1</sup> body weight per day). Similar edible conductive oleogels have been characterized in a previous work.<sup>[27]</sup>

A conductive sphere with an average diameter of  $7.0 \pm 0.3$  mm (average weight =  $192.8 \pm 36.4$  mg) was obtained by molding. To realize the edible electrodes, an ethyl cellulose (E 462) film was first prepared by casting. An edible gold foil (E 175) was laminated onto the film, and then cut to form  $0.5 \times 4$  cm<sup>2</sup> electrodes. The conductive mass and the two electrodes were enclosed in an edible cavity, namely a 000 gelatin (E 441) capsule. A spacer made from Haribo gummy bears was placed between the electrodes to keep them in place and avoid unwanted contact. The process for the fabrication of the sensor does not require specialized equipment and occurs at relatively low temperature (80 °C), ensuring an environmentally friendly approach. Details for the preparation of each element are reported in the “Experimental Section.”

For testing purposes, the edible sensor was interfaced with standard electronics in a voltage divider configuration using a 1.8 M $\Omega$  pull-down resistor and a 3.3 V supply (Figure 1c). The resistance of the sensor in the ON state was in the order of tens of k $\Omega$  (Video S1, Supporting Information). In this configuration, the ON and OFF states of the sensor are transduced to high or low voltage, respectively. The sensor output was measured during

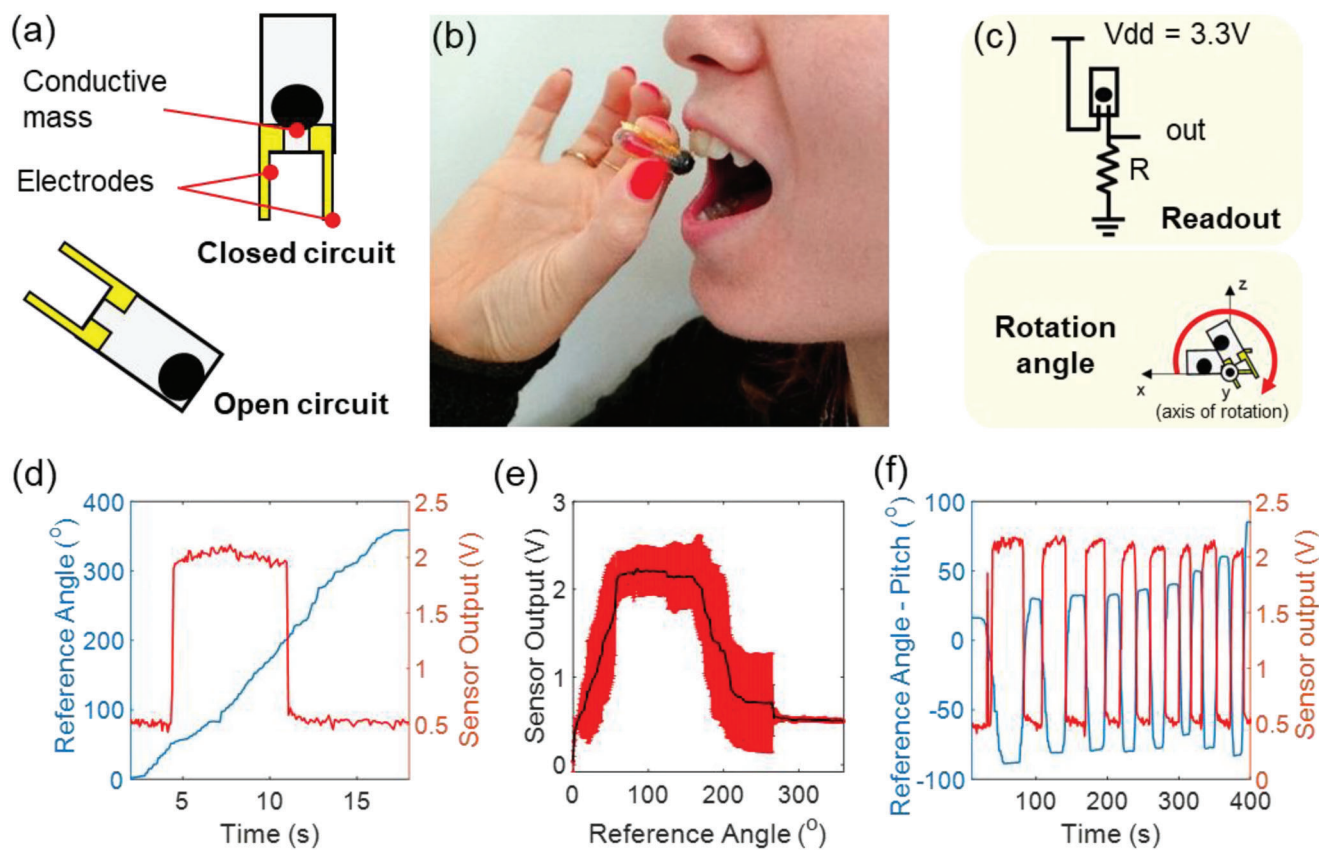


**Figure 1.** a) Working principle of the bistable tilt sensor. b) Fully edible implementation of the bistable tilt sensor. c) Readout and rotation axis for sensor characterization using a voltage divider with a pull-down resistor of 1.8 M $\Omega$  and a voltage supply of 3.3 V. d) Typical response of the sensor (red) while the reference angle is linearly increased over time (blue). e) Reference angle against average and standard deviation of the sensor output over ten repeated experiments. f) Reference angle (blue) and sensor output (red) over time for eight consecutive 360° rotations.

uniaxial rotations, and the reference angle was measured with commercial inertial sensors (Figure S1c, Supporting Information). As the rotation angle is increased (blue curve in Figure 1d), the sensor output (red curve in Figure 1d) switches to the ON state at a certain threshold angle and remains in such a state until a further increase of the rotation angle opens the circuit (OFF state). Ten experiments were performed by rotating the sensor between 0° and 360°, and a sensor characteristic illustrating sensor output against reference angle was obtained (Figure 1e; Figure S1d,e, Supporting Information). Data show that the sensor maintains the ON state from 57° to 162° (ON-state window length: 105°). The change of sensor state is clearly detectable and can be easily identified using numerical methods (e.g., derivative in Figure S1f in the Supporting Information). To assess the repeatability of sensor readings, the same setup was used to detect iterative 360° rotations with the same sensor (eight full rotations in Figure 1f). Results show that the sensor consistently follows the reference angle and reliably detects each rotation. Although constituted of edible materials, the sensors can provide a detectable output after at least 259 days (see Figure S1h in the Supporting Information). The sensor was also successfully operated using the edible battery developed by Ilic et al.<sup>[34]</sup> (see Figure S1i in the Supporting Information), thus demonstrating its compatibility with edible power sources.

### 3. Sensor Array Integration and Validation

To validate the tilt sensor functionality in a robotic system, a partially edible rolling robot was developed with locomotion performance similar to conventional nonedible ones (Table S1, Supporting Information). The robot uses data from the array of tilt sensors to perceive its orientation and actuate the correct actuator to start or maintain the rolling motion in a closed loop. The robot (Figure 2a) is composed of i) an array of edible tilt sensors, ii) an edible wheeled structure, iii) an array of edible actuators, iv) standard electronics, and v) standard pneumatics. An external control hub (i.e., a mobile phone) was used to receive and send data wirelessly via Bluetooth during testing. Several components including the electronic circuit, the microcontroller, pneumatic components, and the battery are inedible in the current implementation (see the “Experimental Section” for a detailed description).

An array of six edible sensors was positioned along the circumference (“S0–S5” in Figure 2a) of the edible frame. As such, each sensor has a 60° angular displacement with respect to the next one. The number of tilt sensors is set to six to avoid ambiguity in orientation sensing (see Section S5 in the Supporting Information). With a weight of 4.2 g (excluding wires), sensors provide an estimated 14.3 kcal ( $\approx 0.06$  MJ) from 0.5 g of carbohydrate, 2.1



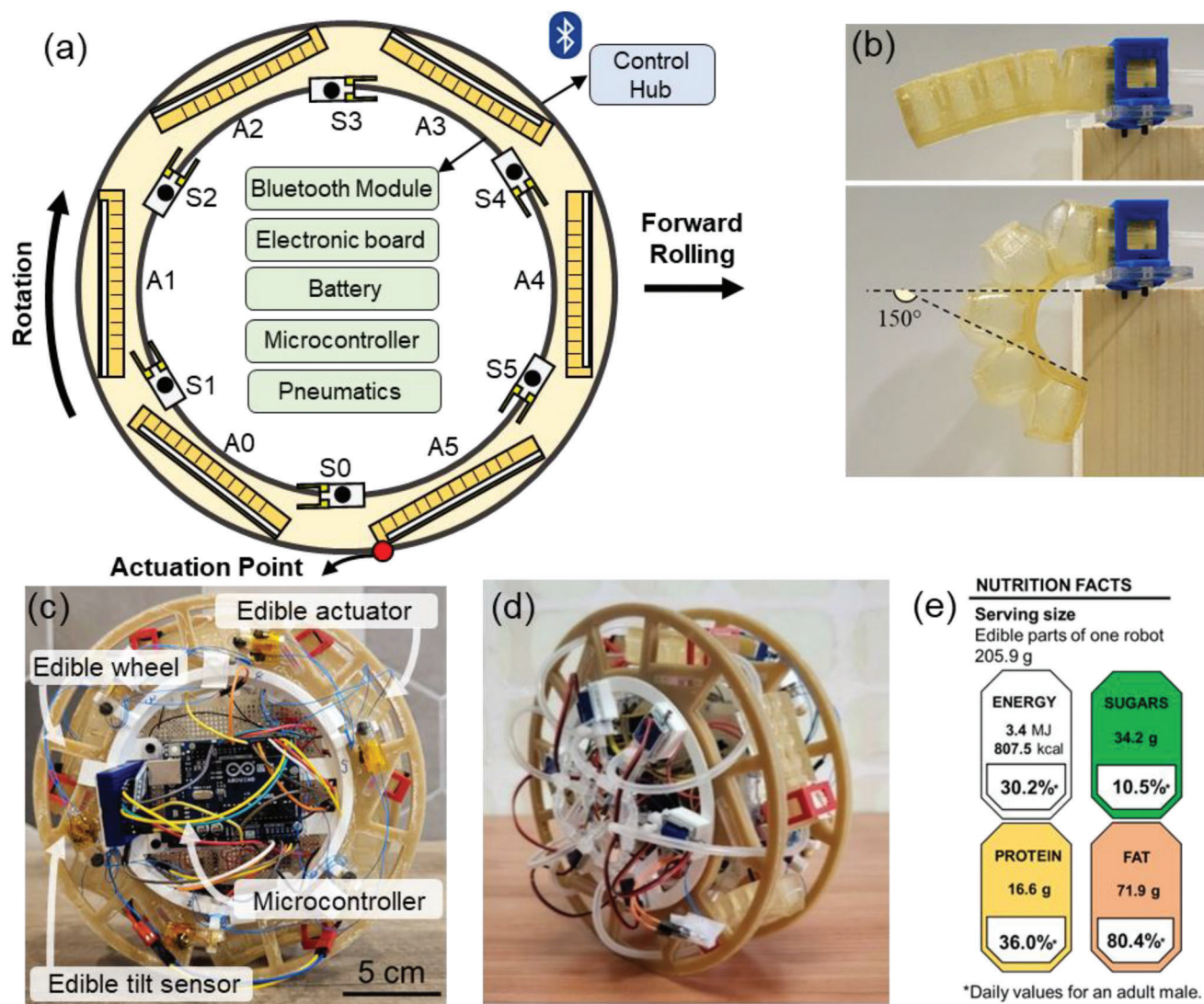


**Figure 2.** a) Architecture of the robot showing the location of the components. b) Actuator in unpressurized state (top) and actuator in pressurized state (22 kPa) with a maximum bending angle of 150° (bottom). c,d) Implementation of the robot (both sides). e) Nutrition facts for one rolling robot. Daily percentage values are calculated according to the European Food Safety Authority (EFSA) dietary recommendations for one adult male with a body weight of 70 kg and with an average level of physical activity (PAL = 1.6).<sup>[62,63]</sup>

g of protein, and 0.5 g of fat. The edible wheel with a diameter of 19.85 cm was made of an oleogel composite<sup>[61]</sup> composed of ethyl cellulose, carnauba wax (E 903), and olive oil in 2:1:6 mass ratio. The structure has a weight of 100.34 g and a nutritional value of 590.7 kcal ( $\approx 2.5$  MJ) from 71.4 g of fat. An array of six gelatin actuators adapted from previous works<sup>[8]</sup> (Figure 2b; Figure S2b, Supporting Information) was similarly placed around the robot circumference (“A0–A5” in Figure 2a). Actuators weigh 101.33 g and provide about 202.5 kcal ( $\approx 0.85$  MJ) from 33.7 g of carbohydrates and 14.5 g of proteins. The final implementation of the robot is illustrated in Figure 2c,d.

Altogether, the total mass of the robot, including nonedible components, is 566.23 g, resulting in a 36.4% ratio of edible materials providing 807.5 kcal ( $\approx 3.4$  MJ), from 34.2 g of carbohydrate, 16.6 g of protein, and 71.9 g of fat (Figure 2e).<sup>[62,63]</sup> Additional de-

tails are discussed in the “Experimental Section” and in Sections S4–S7 (Supporting Information). The autonomous operation of the robot requires the identification of a control system that translates a sensory state (pattern of sensor outputs) into action space (pattern of actuator activations). We identified a set of six orientation states, each corresponding to the activation of one of the six actuators, as defined in Figure 3a.

To demonstrate that the sensor array can uniquely define these six states, the robot was first tested in static conditions. As such, the robot was brought in each of the six states and the sensory state was acquired for five full consecutive cycles. Data from each sensor were converted into a logic state (ON = 1, OFF = 0) using a threshold set to half of the sensor dynamic (Figure 3b for sensor 5; Figure S3 in the Supporting Information for full dataset). The 6bit binary code produced by concatenating the logic values from

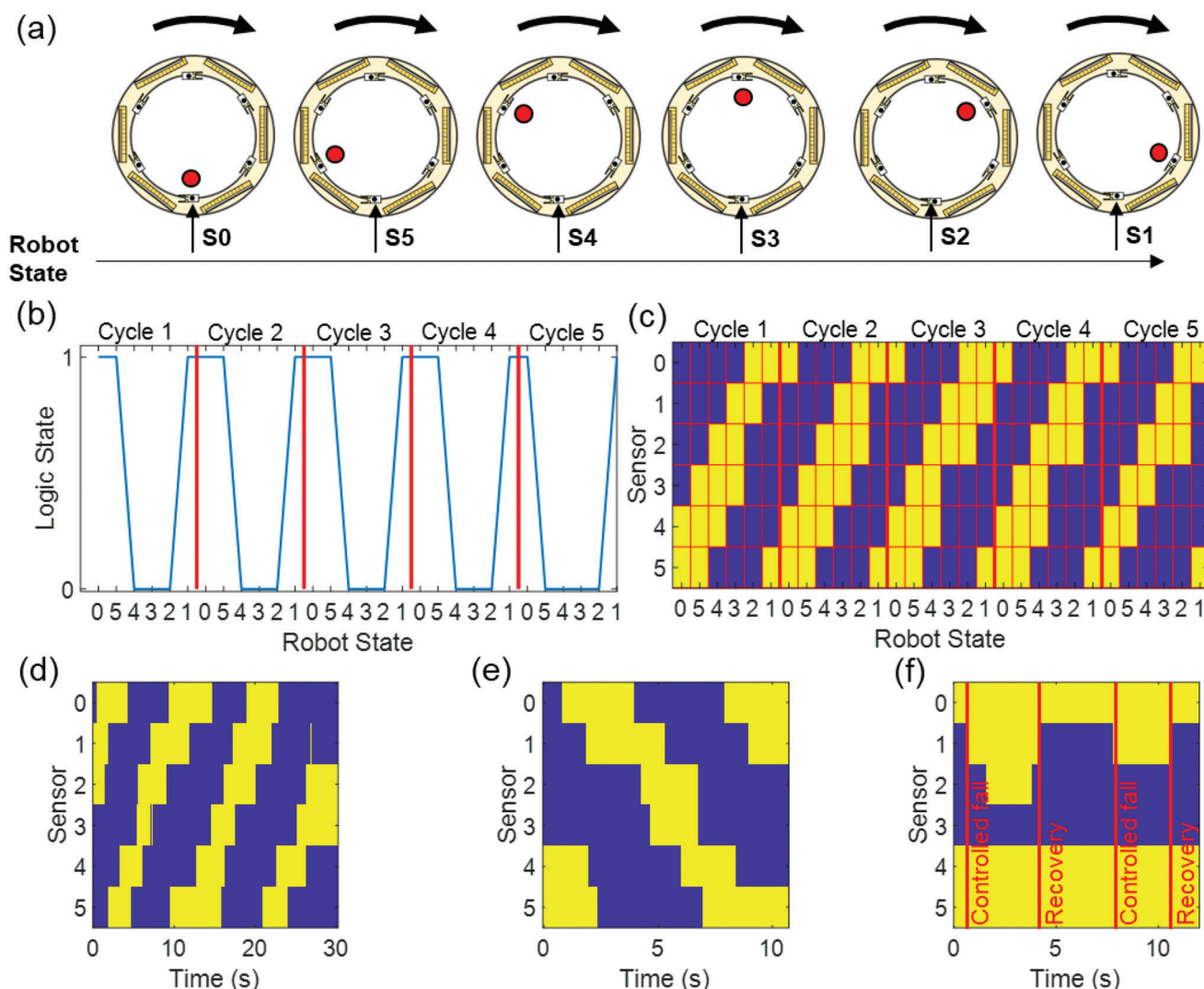


**Figure 3.** Data obtained during passive rolling. a) Definition of the six robot states expected during rolling. b) Logic state from a single sensor (S5) for five rotation cycles. c) Output from the sensor array (logic states—blue/yellow: sensor is OFF/ON) during five rotation cycles measured in static conditions. d) Output from the sensor array during forward rolling over time. e) Output from the sensor array during backward motion over time. f) Output from the sensor array during simulated fall and recovery.

the sensors provided patterns that are unique for each of the robot states (Figure 3c) and were used to define a look-up table (Table S2, Supporting Information).

The sensor array was then tested in dynamic conditions without actuation (passive rolling). When the robot was in a steady-state position, sensor outputs were virtually constant over time (Figure S4a, Supporting Information). Forward rolling was then induced (Figure 3d). The sensor pattern was matching the robot state look-up table. However, due to the dynamic conditions, an increase of the noise level was observed. Backward rolling was also induced, yielding to systematically reversed patterns (Figure 3e). Although the robot was not designed to actively execute backward rolling using the actuators, this test shows that sensors can provide information on the rolling direction. Fall events from resting position were also induced (Figure S5a, Supporting Information). After the fall event, the sensor outputs

identified patterns not-reachable during rolling (Figure 3f). The sensor outputs recovered to valid patterns when the robot was brought to its original position. Therefore, sensor data which are inconsistent with the rolling motion can be used to identify fall events or malfunctioning. Autonomous operation was then demonstrated (Figure 4a; Videos S2–S4, Supporting Information). We show that the array of sensors is successful in perceiving the orientation of the robot in real time, which in turn activates the correct actuators in sequence to start and maintain the forward rolling movement (Figure 4c). A specific test protocol (reported in the “Experimental Section”) was defined to quantify the success rate in perceiving the orientation and addressing the correct actuator to start or maintain the forward rolling. Overall, we recorded an 85.4% success rate (Figure 4b; Table S3, Supporting Information). Data from the six sensors can also be used to estimate the translational speed of the robot (Figure 4d,e; Video

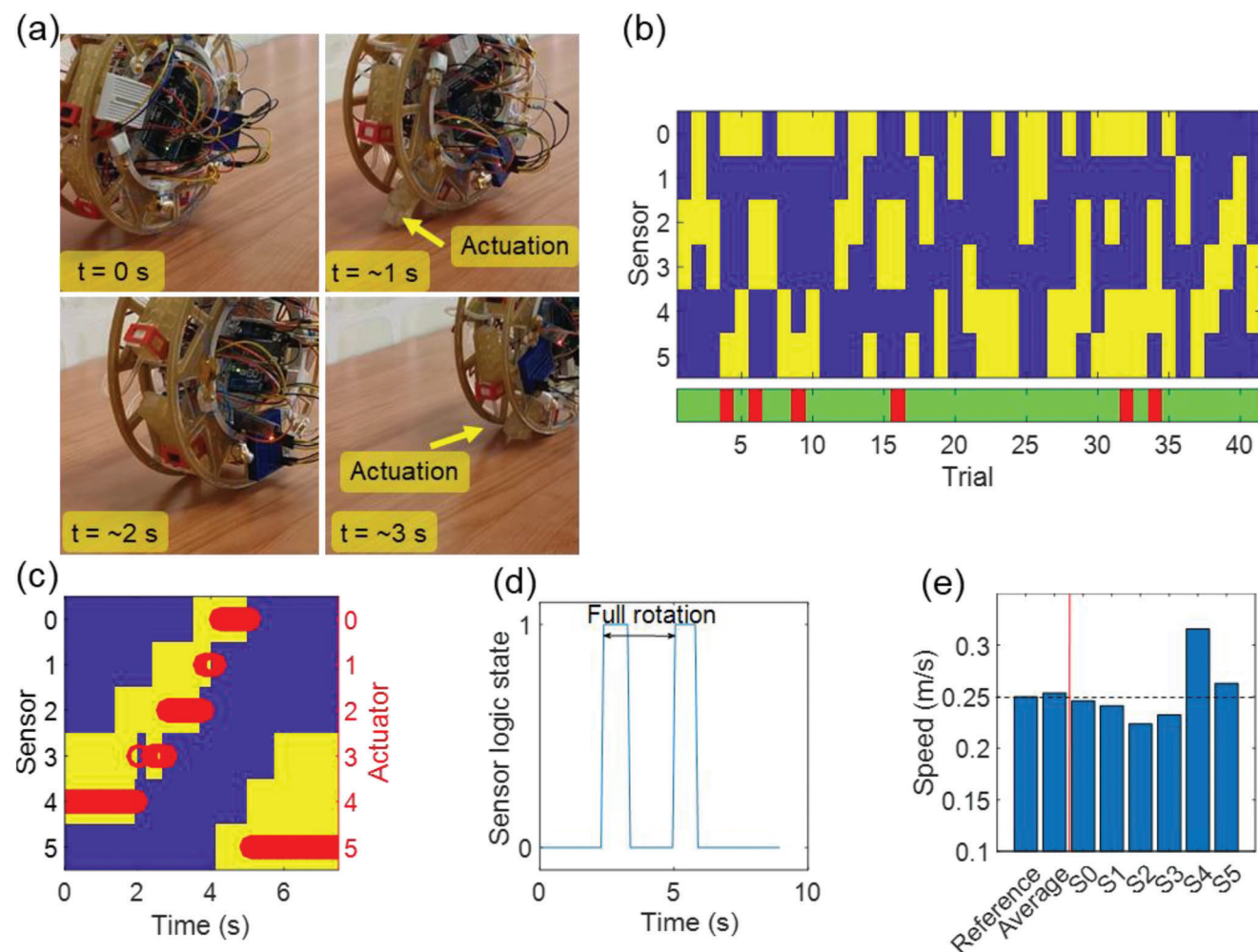


**Figure 4.** Data obtained during active rolling. a) Photographs of the robot during autonomous rolling. b) Estimation of actuation success rate over 41 trials. c) Data from sensors and actuators (in red) during autonomous rolling. Red markers identify the activation of the respective actuator. d) Data from a single sensor during rolling for translational speed estimation. e) The translational speed of the robot estimated using single sensors and their average compared to the reference.

S5, Supporting Information). Data showed a good agreement between the translational speed measured using the embedded edible sensors ( $0.254 \pm 0.030 \text{ m s}^{-1}$ ) and an external camera ( $0.25 \text{ m s}^{-1}$ ). Additional data are reported in Sections S7–S9 (Supporting Information).

## 4. Conclusions

We described the first edible tilt sensor that can provide information on the orientation state of any rotational system. Starting from a well-known bistable tilt sensor architecture, we replaced each material with an edible equivalent using a simple fabrication process. Repeatable operation of the edible tilt sensor was validated against standard sensors during multiple controlled rotations. Besides being fully edible, the sensor does not require a complex readout circuit, can operate in a direct current regime, and could be digitized using a single inverter. Also the sensor virtually dissipates zero current in the OFF state (open circuit) can

potentially be operated at a very low voltage, and can be easily used in an array configuration.

We validated the edible sensor functionality in a proof of principle and partly eatable rolling robot. Our implementation represents the first integration of edible sensors, edible actuators, and edible structural components into an autonomous robot. Several edible materials were used in the integration of the robot, such as gelatin, edible gold leaves, ethyl cellulose, gummy bears, activated carbon, sunflower and olive oil, beeswax, and carnauba wax, resulting in a nutritional value of 807.5 kcal ( $\approx 30\%$  of the daily intake for an adult male), an unprecedented feature for autonomous robots. We showed that, using data from the edible sensors, the robot can estimate its orientation and engage the appropriate edible actuator to sustain continuous rolling motion, detect forward and backward movement. Furthermore, the sensor data can be used to estimate the translational speed of the robot and ultimately detect falls or inconsistent orientation. The actuation success rate of 85.4% could be improved by numerical regression methods, such as simple neural networks, as



discussed in Section S9 (Supporting Information). We believe that the technology and the vision herein illustrated can pave the way to a new class of edible devices with applications spanning from medicine to food quality control, including novel educational and recreational food experiences. The positive environmental impact of edible technologies can also extend to other applications, where processes and materials herein developed will enable the use of edible alternatives.

## 5. Experimental Section

**Ethyl cellulose** (48.0–49.5% w/w ethoxyl basis), beeswax (refined), activated carbon (Supelco 05105), gelatin (from porcine skin), and absolute ethanol were purchased from Sigma-Aldrich. Glycerol (99%) was purchased from Abcr. Edible gold foils ( $4 \times 4 \text{ cm}^2$ ) were purchased from Kinno. Sunflower oil (Esselunga) and olive oil (Bertolli) were purchased from local supermarkets. Gelatin Capsule (000) was purchased from JG Supplements LTD.

**Electrodes:** Ethyl cellulose was dissolved in ethanol, obtaining a solution with a concentration of  $20 \text{ g L}^{-1}$ . About 30 mL of the solution was then poured into a Petri dish (diameter = 9.5 cm), and the solvent was evaporated in a static oven at  $60^\circ\text{C}$  for 17 h. Once formed, the ethyl cellulose film was removed from the Petri dish, with a razor blade and water. The flat side of the ethyl cellulose film was wet with ethanol and placed onto an edible  $4 \times 4 \text{ cm}^2$  gold leaf. The so-gold-laminated films were dried in air for a few hours to evaporate ethanol, placing a weight on top (e.g., a small Petri dish) to avoid the formation of wrinkles, and then were vacuum-dried for 17 h in a vacuum chamber. Finally,  $0.5 \times 4 \text{ cm}^2$  stripe electrodes were cut from gold-laminated ethyl cellulose films.

**Conductive Mass:** Beeswax was first melted onto a hotplate at  $80^\circ\text{C}$ . Beeswax was then mixed with sunflower oil with a 3:1 weight ratio by magnetic stirring for 10 min. Subsequently, activated carbon was added in a 30% weight ratio with respect to the oleogel matrix and mixed using a magnetic stirrer for 10 min at  $80^\circ\text{C}$ . The material was then transferred into a commercially sourced semispherical silicon mold and cooled down at room temperature for 30 min. To join two half-spheres, a glass slide was heated to  $80^\circ\text{C}$  and was used to partially melt the flat side of both the half spheres. The two half-spheres were then brought to contact. In the final implementation of the partially edible robot, the conductive sphere was wrapped using a gold foil to further reduce its resistance and improve the signal-to-noise ratio of the sensor output.

**Gelatin Actuator:** The fabrication process was almost the same as the previously developed edible pneumatic actuator,<sup>[8]</sup> but with different dimensions. Gelatin, glycerol (99%), and distilled water were mixed in 1:2:3 ratio and stirred overnight at  $65^\circ\text{C}$ . The upper layer was molded and dried inside a fume hood overnight. After that, the same gelatin solution was casted on an acrylic plate, and the demolded upper layer was placed on the casted bottom layer to bond the upper and bottom layers. As a final step, the bonded structure was cured overnight in a fume hood at room temperature.

**Edible Structural Components:** The edible wheel was made of an edible oleogel composite.<sup>[58]</sup> This composite was prepared by mixing ethyl cellulose, food-grade carnauba wax, and olive oil in 2:1:6 mass ratio followed by heating at  $150^\circ\text{C}$  during 20 min. As shown in Figure S8 (Supporting Information), the heated oleogel solution was poured onto a silicone mold (Smooth-Sil 940, Smooth-On), which was designed to produce an edible wheel in a desired shape. Since the heated oleogel solution would quickly solidify at room temperature, uniformly casting the solution in the silicone mold was challenging, and usually generated an irregular surface (step 2 in Figure S8 in the Supporting Information). For this reason, the entire mold casted with the oleogel was reheated inside a cooking oven at  $150^\circ\text{C}$  until the casted material was re-melted. After that, the excess oleogel was manually removed by using a spreading knife (steps 3 and 4 in Figure S8 in the Supporting Information) while it was still in liquid state. Then the mold was cooled down at room temperature for at least 1 h, and the edible wheel was demolded (steps 5 and 6 in Figure S8 in the Supporting In-

formation). The described molding process can produce a planar oleogel structure with a good surface finish (step 6 in Figure S8 in the Supporting Information). The thickness and density of the edible wheel were 5 mm and  $0.92 \text{ g cm}^{-3}$ , respectively.

**Sensor Characterization:** The sensor was connected to the readout circuitry using silver epoxy (MG Chemicals 8331S). The sensor and the readout circuitry were inserted into a rigid custom holder. The output of the voltage divider was connected to a microcontroller (STM32 Nucleo-64 STMicroelectronics, CPU ARM Cortex M4F) and digitized using the embedded 12-bit ADC. The microcontroller was also used to supply the voltage required for the operation of the circuit. The microcontroller was connected to a laptop (HP EliteBook x360 830 G6) via USB. In the same custom holder containing the sensor and readout circuitry, a smartphone with inertial sensors (Huawei P30) was also included. Azimuth, pitch, and roll data from the smartphone were sent to the same laptop via Wi-Fi using the Matlab Mobile App. A custom Matlab script running on the laptop was used to acquire and store at the same time data from the sensor via the microcontroller and reference angle data from the smartphone with a sampling time of  $108 \pm 10 \text{ ms}$ . Data were collected while manually rotating the holder clockwise with an average angular speed of  $22.86 \pm 6.41^\circ/\text{s}$ . The y-axis was assumed as the rotational axis and the sensor was positioned as in Figure 1c. The holder was free to perform full  $360^\circ$  rotations. Figure S1c (Supporting Information) illustrates a schematic diagram of the sensor characterization setup.

**Integration:** To connect the edible sensor to a standard wire, an edible electrically conductive composite made of beeswax and activated carbon in a 30% weight ratio was formulated (see Figure S2c,d in the Supporting Information). To prepare the composite, beeswax was melted at  $80^\circ\text{C}$  and stirred using a magnetic stirrer for 10 min. Then, activated carbon was added in the desired ratio. The melted composite was then used as conductive adhesive material to attach the electrodes to a standard wire. Once cooled down, the composite material showed good adhesion and mechanical strength. The electronics was implemented using a custom electronic board with discrete components for readout circuits connected to a microcontroller (Arduino Uno Rev3) mounting a ATmega328P-16 processor. The microcontroller board was also connected to a Bluetooth 4.0 BLE module (AT-09 BLE) to enable communication with the external control hub (an external electronic device with a commercial serial Bluetooth terminal app running—a smartphone Samsung Galaxy Z Flip 4) and controlled seven metal-oxide-semiconductor field effect transistors (MOSFET) (PSMN1R8-30PL, Nexperia) to switch on and off a pump (SP 100 EC-LC, Schwarzer Precision) and six 3-way solenoid valves (Fa0520E, Adafruit). Each valve can individually drive an edible actuator. The actuator can bend up to  $150^\circ$  in unloaded case with an applied air pressure of 22 kPa (as in Figure 2b). To avoid over-pressurization of the actuators, a pressure sensor (ABP series, Honeywell) was also installed and communicated with the Arduino via SPI (serial peripheral interface) protocol. The number and the location of the actuators were experimentally defined and tuned to ensure continuous rolling motion. The activation of a single actuator at a time was sufficient to cause a rolling motion of the robot. Each edible sensor was first connected to a voltage divider circuit (see Figure S2a in the Supporting Information), and its output voltage was then connected to an analog-to-digital converter (ADC) port of Arduino, which provided six ADCs in 10-bit resolution. Electronic and pneumatic components were powered by a battery (7.6 V, 500 mAh, Turnigy). The output current was measured by a current sensor (INA219, Reichelt Elektronik) to compute power consumption of the robot. As illustrated in Figure S9 (Supporting Information), several inedible components were still in use. The fixtures to hold edible sensors, edible actuators, and electronics (including the pneumatic hardware) were 3D-printed with acrylonitrile butadiene styrene (ABS). The rigid frame connecting the two edible wheels was made of a 3 mm thick, laser-cut acrylic sheet. A schematic of the entire connections is reported in Figure S2i (Supporting Information).

The microcontroller board was equipped with a custom firmware to collect data from the sensors, perceive the orientation, and activate the suitable actuator to achieve autonomous rolling. At each iteration of the firmware, data from the six sensors were sequentially digitized (sampling time:  $87 \pm 1 \text{ ms}$ ) and sent to the control hub, together with information

on the actuators state. Using a threshold set to half of the sensor dynamic, data from each sensor were numerically converted into a logic state (ON = 1, OFF = 0). The six resulting logic values were concatenated from S0 to S5 to create a 6 bit binary code. With six sensors,  $2^6 = 64$  codes are possible. Codes were associated with robot states by defining a look-up table. The table identifies valid and not-reachable states, which are defined as positions which are compatible or incompatible with the rolling motion, respectively. When the robot recognizes a valid state, it activates the correct actuator to enable or continue a forward rolling motion as defined in the look-up table. To activate/deactivate the actuators, seven digital outputs were used to enable/disable (1/0) the six pneumatic valves and the pump (Figure S2i, Supporting Information). If the robot recognizes a not-reachable state, it deactivates all the actuators and sends an alert message to the control hub. The look-up table (Table S2, Supporting Information) and a flow chart of the algorithm are reported in Figure S2j (Supporting Information). The final implementation of the robot had a diameter of 19.85 cm where the electronic and pneumatic components and the battery were positioned at the center of the wheeled frame to balance the robot during rotation (Figure S2e–h, Supporting Information).

**Validation:** In all the testing phases, data were sent to the external hub in real time using Bluetooth. A mobile phone running a commercial app for serial communication was used as external hub. Data were then exported and analyzed using Matlab. To test the robot in static conditions (Figure 3b,c), data were recorded in specific resting positions of the robot. For each robot state, two specific 6 bit codes were observed. This was due to variations of the threshold angle for different devices and different events. As such, both the 6 bit codes were considered valid and referred to a single robot state. All other 6 bit codes not observed during this phase were considered not-reachable states. To test the robot during passive rolling (Figure 3d–f), a rotation was manually induced, and actuators were not enabled from the firmware. The sensor pattern was matching the robot state look-up table. To test fall events (Figure 3f), starting from a valid state the robot was laid down as in Figure S5a (Supporting Information). The robot was then brought back in a valid position after a few seconds. To test the success rate in determining the correct state of the robot (Figure 4b), a custom protocol was defined. The robot was brought into one of the six states using a random number generation. A full clockwise rotation was performed before any test to ensure independent data. Then, the robot was started, and data from the first actuation were recorded. An actuation was considered successful only if the actuation started the forward rolling of the robot. Any other case was considered a failed actuation. The experiment was repeated 41 times. Each repetition was herein referred to as a trial. Table S3 (Supporting Information) reports the details of this testing phase. Failures were mainly related to false positives or false negatives of the sensors or actuators (see the Supporting Information). To demonstrate that sensory data can be used to estimate the translational speed of the robot (Figure 4d,e), the firmware of the robot was modified to perform only one initial actuation. Two consecutive rising edge of a sensor output identify a full rotation. The circumference of the robot was 62.3 cm. As such, the translational speed was obtained by dividing the circumference of the robot with the time required for one full rotation. The reference speed was obtained by video recording the robot using a mobile phone (Huawei P30). The video was then processed using Matlab to estimate the speed of the robot.

## Supporting Information

Supporting Information is available from the Wiley Online Library or from the author.

## Acknowledgements

V.F.A. and B.K. contributed equally to this work. V.F.A., B.K., G.C., V.G., D.F., and M.C. acknowledge the support of the European Union's Horizon 2020 research and innovation program under Grant Agreement #964596 "ROBOFOOD". I.K.I. and M.C. acknowledge the support of the

European Research Council (ERC) under the European Union's Horizon 2020 research and innovation programme "ELFO", Grant Agreement #864299. P.C. acknowledge funding from the Marie Skłodowska-Curie actions (project name: BioConTact, Grant Agreement #101022279) under the European Union's Horizon 2020 research and innovation programme.

## Conflict of Interest

The authors declare no conflict of interest.

## Data Availability Statement

The data that support the findings of this study are available from the corresponding author upon reasonable request.

## Keywords

activated carbon, edible electronics, edible robotics, edible sensors, green robotics, sustainability

Received: June 16, 2023

Published online:

- [1] F. Hartmann, M. Baumgartner, M. Kaltenbrunner. *Adv. Mater.* **2020**, 33, 2004413.
- [2] X. Wu, P. Steiner, T. Raine, G. Pinter, A. Kretinin, C. Kocabas, M. Bissett, P. Cataldi, *Adv. Electron. Mater.* **2020**, 6, 2000232.
- [3] World Economic Forum. *A New Circular Vision for Electronics. Time for a Global Reboot*, [https://www3.weforum.org/docs/WEF\\_A\\_New\\_Circular\\_Vision\\_for\\_Electronics.pdf](https://www3.weforum.org/docs/WEF_A_New_Circular_Vision_for_Electronics.pdf) (accessed: March 2023).
- [4] Empire State Realty Trust, *Empire State Building Fact Sheet*, <https://www.esbny.com/> (accessed: March 2023).
- [5] M. Shahabuddin, M. N. Uddin, J. I. Chowdhury, S. F. Ahmed, M. Mofijur, M. A. Uddin, *Int. J. Environ. Sci. Technol.* **2023**, 20, 4513.
- [6] P. Cataldi, O. Condurache, D. Spirito, R. Krahne, I. S. Bayer, A. Athanassiou, G. Perotto, *ACS Sustainable Chem. Eng.* **2019**, 7, 12544.
- [7] S. Ceron, A. Kurumunda, E. Garg, M. Kim, T. Yeku, K. Pctersen, in *2018 IEEE Int. Conf. on Robotics and Automation (ICRA 2018)*, IEEE, Brisbane, Australia, May 2018.
- [8] J. Shintake, H. Sonar, E. Piskarev, J. Paik, D. Floreano, in *2017 IEEE/RSJ Int. Conf. on Intelligent Robots and Systems (IROS)*, IEEE, Vancouver, BC, Canada, September 2017.
- [9] J. Hughes, D. Rus, in *3rd IEEE Int. Conf. on Soft Robotics (RoboSoft)*, IEEE, New Haven, CT, USA, May–July 2020.
- [10] I. K. Ilic, L. Lamanna, D. Cortecchia, P. Cataldi, A. Luzio, M. Caironi, *ACS Sens.* **2022**, 7, 2995.
- [11] B. Kwak, J. Shintake, L. Zhang, D. Floreano, in *IEEE/RSJ Int. Conf. on Intelligent Robots and Systems (IROS)*, IEEE **2022**, pp. 1802–1809, <https://doi.org/10.48550/arXiv.2211.04149>.
- [12] J. Llacer-Wintle, A. Rivas-Dapena, X. Chen, E. Pellicer, B. J. Nelson, J. Puigmartí-Luis, S. Pané, *Adv. Mater.* **2021**, 33, 2102049.
- [13] S. Miyashita, S. Guitron, K. Yoshida, S. Li, D. D. Damian, D. Rus, in *2016 IEEE Int. Conf. on Robotics and Automation (ICRA)*, IEEE, Stockholm, May 2016.
- [14] R. Tan, X. Yang, H. Lu, L. Yang, T. Zhang, J. Miao, Y. Feng, Y. Shen, *Matter* **2022**, 5, 1277.
- [15] S. R. Goudi, I. C. Yasa, X. Hu, H. Ceylan, W. Hu, M. Sitti, *Adv. Funct. Mater.* **2020**, 30, 2004975.
- [16] Y. Yamada, *IEEE Robot. Autom. Lett.* **2021**, 6, 3777.



- [17] M. Baumgartner, F. Hartmann, M. Drack, D. Preninger, D. Wirthl, R. Gerstmayr, L. Lehner, G. Mao, R. Pruckner, S. Demchyshyn, L. Reiter, M. Strobel, T. Stockinger, D. Schiller, S. Kimeswenger, F. Greibich, G. Buchberger, E. Bradt, S. Hild, S. Bauer, M. Kaltenbrunner, *Nat. Mater.* **2020**, 19, 1102.
- [18] S. D. Cezan, H. T. Baytekin, B. Baytekin, *Soft Rob.* **2020**, 7, 444.
- [19] J. Rossiter, J. Winfield, I. Ieropoulos, *Proc. SPIE* **2016**, 9798, 97981S.
- [20] V. F. Annesse, D. De Venuto, C. Martin, D. R. S. Cumming, in *21st IEEE Int. Conf. on Electronics, Circuits and Systems*, IEEE, Marseille, France, December 2014.
- [21] C. Hu, V. F. Annesse, S. Velugotla, M. Al-Rawhani, B. C. Cheah, J. Grant, M. P. Barrett, D. R. S. Cumming, *IEEE Trans. Biomed. Eng.* **2020**, 67, 2417.
- [22] E. H. Rumley, D. Preninger, A. S. Shomron, P. Rothenmund, F. Hartmann, M. Baumgartner, N. Kellaris, A. Stojanovic, Z. Yoder, B. Karrer, C. Keplinger, M. Kaltenbrunner, *Sci. Adv.* **2023**, 9, eadf5551.
- [23] A. Heiden, D. Preninger, L. Lehner, M. Baumgartner, M. Drack, E. Woritzka, D. Schiller, R. Gerstmayr, F. Hartmann, M. Kaltenbrunner, *Sci. Rob.* **2022**, 7, eabk2119.
- [24] H. A. Leslie, M. J. M. van Velzen, S. H. Brandsma, A. D. Vethaak, J. J. Garcia-Vallejo, M. H. Lamoree, *Environ. Int.* **2022**, 163, 107199.
- [25] M. Shen, B. Song, G. Zeng, Y. Zhang, W. Huang, X. Wen, W. Tang, *Environ. Pollut.* **2020**, 263, 114469.
- [26] V. C. Shruti, G. Kutralam-Muniasamy, *Sci. Total Environ.* **2019**, 697, 134139.
- [27] P. Cataldi, L. Lamanna, C. Bertei, F. Arena, P. Rossi, M. Liu, F. Di Fonzo, D. G. Papageorgiou, A. Luzio, M. Caironi, *Adv. Funct. Mater.* **2022**, 32, 2113417.
- [28] K. Chen, L. Yan, Y. Sheng, Y. Ma, L. Qu, Y. Zhao, *ACS Nano* **2022**, 16, 15261.
- [29] A. S. Sharova, M. Caironi, *Adv. Mater.* **2021**, 33, 2103183.
- [30] M. Saha, S. M. Nawaz, B. K. Keshari, A. Mallik, *ACS Appl. Bio Mater.* **2022**, 5, 833.
- [31] S. Mao, B. Sun, T. Yu, W. Mao, S. Zhu, Y. Ni, H. Wang, Y. Zhao, Y. Chen, *New J. Chem.* **2019**, 43, 9634.
- [32] G. Saravanavel, V. Upadhye, S. Praneeth, S. John, G. S. Wyatt-Moon, K. R. Gunashekar, A. J. Flewitt, S. Sambandan, *IEEE Journal on Flexible Electronics* **2023**, <https://doi.org/10.1109/JFLEX.2023.3273183>.
- [33] L. Lamanna, G. Pace, I. K. Ilic, P. Cataldi, F. Viola, M. Friuli, V. Galli, C. Demitri, M. Caironi, *Nano Energy* **2023**, 108, 108168.
- [34] I. K. Ilic, V. Galli, L. Lamanna, P. Cataldi, L. Pasquale, V. F. Annesse, A. Athanassiou, M. Caironi, *Adv. Mater.* **2023**, 35, 2211400.
- [35] D. Lee, B. Chua, *ACS Appl. Mater. Interfaces* **2021**, 13, 43984.
- [36] A. Keller, D. Benz, M. Panhuis, *MRS Online Proc. Libr.* **2015**, 1795, 27.
- [37] S. Tian, Y. Xing, Y. Long, H. Guo, S. Xu, Y. Ma, C. Wen, Q. Li, X. Liu, L. Zhang, J. Yang, *ACS Appl. Mater. Interfaces* **2022**, 14, 5122.
- [38] B. Kuswandi, N. P. N. Asih, D. K. Pratoko, N. Kristiningrum, M. Moradi, *Packag. Technol. Sci.* **2020**, 33, 321.
- [39] W. Xu, H. Yang, W. Zeng, T. Houghton, X. Wang, R. Murthy, H. Kim, Y. Lin, M. Mignolet, H. Duan, H. Yu, M. Slepian, H. Jiang, *Adv. Mater. Technol.* **2017**, 2, 1700181.
- [40] I. Mallov, F. Jeeva, C. B. Caputo, *J. Chem. Technol. Biotechnol.* **2020**, 97, 830.
- [41] K. Fukada, T. Tajima, M. Seyama, *Adv. Mater. Technol.* **2022**, 7, 2200830.
- [42] C. J. Bettinger, *Hepatobiliary Surg. Nutr.* **2019**, 8, 157.
- [43] V. Ruiz-Valdepeñas Montiel, J. R. Sempionatto, S. Campuzano, J. M. Pingarrón, B. J. Wang, *Anal. Bioanal. Chem.* **2019**, 411, 4597.
- [44] L. D. Chambers, J. Winfield, I. Ieropoulos, J. Rossiter, *Proc. SPIE* **2014**, 9056, 46.
- [45] Y. Huang, Q. Cheng, U. Jeng, S. Hsu, *ACS Appl. Mater. Interfaces* **2023**, 15, 5798.
- [46] A. N. Sardesai, X. M. Segel, M. N. Baumholtz, Y. Chen, R. Sun, B. W. Schork, R. Buonocore, K. O. Wagner, H. M. Golecki, *MRS Adv.* **2018**, 3, 3003.
- [47] R. M. Alexander, *Principles of Animal Locomotion*, Princeton University Press, Princeton, NJ **2003**, <https://doi.org/10.1515/9781400849512>.
- [48] R. H. Armour, J. F. V. Vincent, *J. Bionic Eng.* **2006**, 3, 195.
- [49] K. Ly, J. V. Mayekar, S. Aguasvivas, C. Keplinger, M. E. Rentschler, N. Correll, *IEEE Trans. Rob.* **2022**, 38, 3044.
- [50] K. Gilpin, E. Torres-Jara, D. Rus, *Experimental Robotics. Springer Tracts in Advanced Robotics*, Vol. 79 (Eds: O. Khatib, V. Kumar, G. Sukhatme), Springer, Berlin **2014**, p. 149.
- [51] Y. Sugiyama, S. Hirai, *Int. J. Rob. Res.* **2006**, 25, 603.
- [52] M. Artusi, M. Potz, J. Aristizabal, C. Menon, S. Cocuzza, S. Debei, *IEEE/ASME Trans. Mechatronics* **2011**, 16, 50.
- [53] W.-B. Li, W.-M. Zhang, H.-X. Zou, Z.-K. Peng, G. Meng, *IEEE/ASME Trans. Mechatronics* **2018**, 23, 1630.
- [54] A. Firouzeh, M. Ozmaeian, A. Alasty, A. Iraj Zad, *Smart Mater Struct.* **2012**, 21, 065011.
- [55] J. Sastra, S. Chitta, M. Yim, *Int. J. Rob. Res.* **2009**, 28, 758.
- [56] T. Matsuda, S. Murata, in *Proc. 2006 IEEE Int. Conf. on Robotics and Automation*, IEEE, Orlando, FL, USA, May 2006.
- [57] K. Kim, A. K. Agogino, D. Moon, L. Taneja, A. Toghyan, B. Dehghani, V. SunSpiral, A. M. Agogino, in *IEEE Int. Conf. on Robotics and Biomimetics*, IEEE, Bali, Indonesia, December 2014.
- [58] K. W. Wait, P. J. Jackson, L. S. Smoot, in *IEEE Int. Conf. on Robotics and Automation*, IEEE, Anchorage, AK, USA, May 2010.
- [59] D. Floreano, N. Nosengo, *Tales from a Robotic World: How Intelligent Machines Will Shape Our Future*, The MIT Press, Cambridge, MA **2022**.
- [60] S. Łuczak, M. Ekwirska, *Sensors* **2021**, 21, 1097.
- [61] M. A. Rogers, T. Strober, A. Bot, J. F. Toro-Vazquez, T. Stortz, A. G. Marangoni, *Int. J. Gastron. Food Sci.* **2014**, 2, 22.
- [62] European Food Safety Authority, "Dietary Reference Values | DRV Finder," EFSA, <https://multimedia.efsa.europa.eu/drvs/index.htm> (accessed: March 2023).
- [63] European Food Safety Authority, "Physical Activity Level (PAL)" EFSA, <https://www.efsa.europa.eu/en/glossary/physical-activity-level-pal> (accessed: March 2023).